INORGANIC CHEMISTRY

FRONTIERS

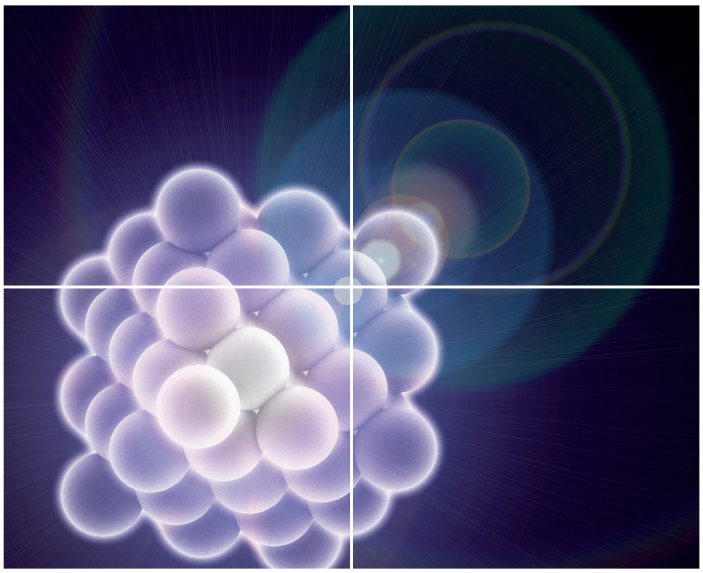

Accepted Manuscript

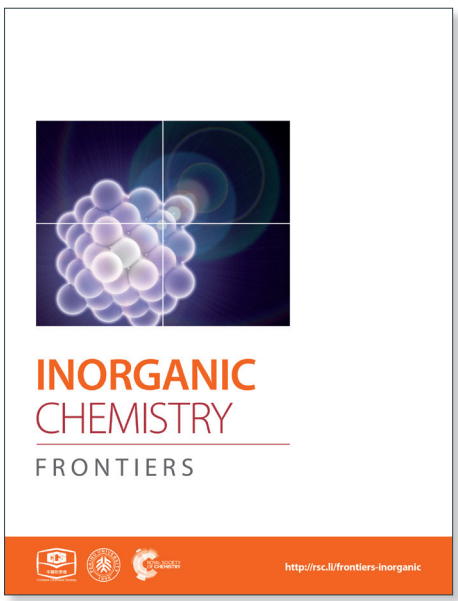

This is an *Accepted Manuscript*, which has been through the Royal Society of Chemistry peer review process and has been accepted for publication.

Accepted Manuscripts are published online shortly after acceptance, before technical editing, formatting and proof reading. Using this free service, authors can make their results available to the community, in citable form, before we publish the edited article. We will replace this *Accepted Manuscript* with the edited and formatted *Advance Article* as soon as it is available.

You can find more information about *Accepted Manuscripts* in the **Information for Authors**.

Please note that technical editing may introduce minor changes to the text and/or graphics, which may alter content. The journal's standard **Terms & Conditions** and the **Ethical guidelines** still apply. In no event shall the Royal Society of Chemistry be held responsible for any errors or omissions in this *Accepted Manuscript* or any consequences arising from the use of any information it contains.

Cite this: DOI: 10.1039/c0xx00000x

www.rsc.org/xxxxxx

ARTICLE TYPE

High quality sulfur-doped titanium dioxide nanocatalysts with visible light photocatalytic activity from non-hydrolytic thermolysis synthesis

Na Li,[a,b] Xinyu Zhang,[a] Weijia Zhou,[c] Zhengqing Liu,[a] Gang Xie,[b] Yaoyu Wang,[b] and Yaping Du*[a,b]

Received (in XXX, XXX) Xth XXXXXXXXX 20XX, Accepted Xth XXXXXXXXX 20XX

DOI: 10.1039/b000000x

A facile non-hydrolytic thermolysis route for monodisperse sulfur doped TiO_2 nanocatalysts is demonstrated. Compared with the as-obtained undoped TiO_2 nanocatalysts, the sulfur doped TiO_2 nanocatalysts present obvious enhanced visible light activation for the degradation of rhodamine B and methylene blue dyes under the artificial visible light (λ = 420–770 nm) irradiation.

Titanium dioxide (TiO_2) is the most widely used photocatalyst in environmental cleaning.[1-4] However, because of its large band gap (E_g = 3.20 eV for anatase), TiO_2 can solely be activated in the ultraviolet (UV) region. The limited UV-driven activity decreases its overall efficiency under natural sunlight irradiation, thus limiting its practical applications. Engineering the band gap of TiO_2 is one of the robust strategies for improving its photocatalytic efficiency, since it can availably extend the absorption from UV to visible-light region. Up to now, many attempts have been made in the field of visible-light-active TiO_2 by introducing various dopants into its crystals lattice, including metal[5] and nonmetal elements.[6] Although metal dopants can give the desired shift of the TiO_2 absorption from UV to visible light region, many of them also serve as recombination centers, which notably reduce the photocatalytic efficiency.[5a,7] Band-gap narrowing by doping nonmetals (such as N, C, S and F) into TiO_2 was recently found to be a more efficient way to yield photocatalysts with high catalytic activity under visible light irradiation.[6] As an important sort of visible light activated doped TiO_2 photocatalysts, S-doped TiO_2 photocatalysts have been receiving intensive interest due to their high photocatalytic activity, structural stability and efficient band gap manipulation.[6c,8,12b]

Various doping strategies have been adopted to achieve S-doped TiO_2 photocatalysts, while most of the S-doped TiO_2 photocatalysts were synthesized by oxidative annealing of TiS_2 or treating the titanium contained precursors in hydrogen sulfide (H_2S) atmosphere at high temperature,[6c,9] besides the energy consumption and intricate setup, the high temperature treatment usually leads to the low surface areas and photocatalytic activities due to the aggregations of catalysts. It is widely recognized that nanosized materials have opened the doors for discovering new properties and applications with respect to their macroscopic counterparts.[10] In recent years, several methods have been developed to prepare S-doped TiO_2 nanocatalysts by a number of research groups. Examples include the catalyzed hydrolysis,[11] hydrothermal,[12] solvothermal synthesis,[13] sol-gel,[14] co-precipitation,[15] ball milling,[16] and supercritical fluid-assisted method.[17]

However, until now, a facile method for the synthesis of high quality (monodisperse, single crystalline, well shaped, and phase pure) dispersible colloidal S-doped TiO_2 nanocatalysts has not been demonstrated yet, which inspires the continuous and systematic exploration. In this paper, for the first time, we report a facile and effective non-hydrolytic thermolysis method for obtaining high quality S-doped TiO_2 nanocatalysts in high boiling solvents, and in-depth investigate the photocatalytic properties of as-obtained nanocatalysts. In comparison with the pure TiO_2 nanocatalysts, the absorption edge shift to visible light region by doping S into the TiO_2 crystal lattice, and thus exhibiting a obvious visible light activation for the degradation of rhodamine B and methylene blue dyes.

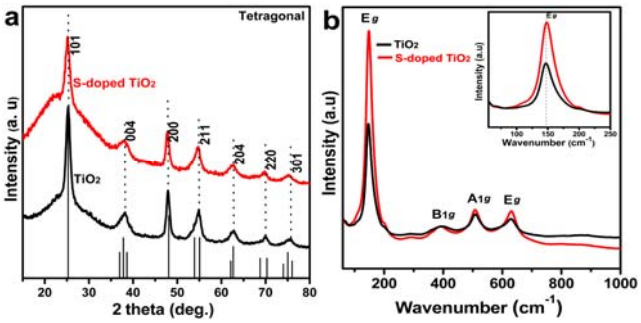

Fig. 1 (a) PXRD patterns of as-synthesized TiO_2 and S-doped TiO_2 nanocrystals. (b) Raman spectra of as-obtained pure TiO_2 and S-doped TiO_2 nanocrystals excited with Ar^+ 514.5 nm, inset is the magnified region of E_g Raman band at 147 cm^{-1}.

The powder X-ray diffraction (PXRD) patterns of as-prepared pure TiO_2 and S-doped TiO_2 nanocrystals are shown in Fig. 1a. The as-synthesized samples exhibit the well-defined diffraction peaks, indicative of a high crystallinity of the sample. All the diffraction peaks are exclusively indexed to anatase phase of TiO_2 (tetragonal structure; JCPDS card no. 21-1272, space group I_{41}/amd) for both pure and S-doped TiO_2 nanocrystals. No diffraction peaks from any other chemical species such as rutile, brookite phase of TiO_2 are detectable. Compared with the pure TiO_2, a systematical peak shift towards low diffraction angles is unambiguously detected in the S-doped TiO_2 nanocrystals (Fig. S1†), suggesting a lattice expansion when introducing S into TiO_2

crystal lattice. Using the least squares refinement of cell dimensions from PXRD data, the calculated crystal lattice parameters are as follows: $a = b = 3.7852$ Å, $c = 9.5139$ Å, $V = 136.3127$ Å^3 for TiO_2 nanocrystals; $a = b = 3.8008$ Å, $c = 9.5212$ Å, $V = 137.5440$ Å^3 for S-doped TiO_2 nanocrystals.

In order to obtain more information about the microstructure of as-obtained S-doped TiO_2 nanocrystals, their room temperature Raman spectra were measured. Group theory predicts the typical anatase TiO_2 has six Raman active modes: $\Gamma=A_{1g} + 2B_{1g} + 3E_g$.[18] Fig. 1b displays the Raman spectrum of as-obtained undoped TiO_2 and S-doped TiO_2 nanocrystals excited with 514.5 nm beam of Ar^+ laser. The Raman spectra of as-obtained nanocrystals presents four bands at 147 cm^{-1} (E_g), 392 cm^{-1} (B_{1g}), 508 cm^{-1} (A_{1g}) and 631 cm^{-1} (E_g). All samples exhibit the characteristic Raman-active modes of the anatase TiO_2 phase, and no detectable signals corresponding to any other titanium and sulfur containing species in the Raman spectra, demonstrating the doped nanocrystals keep the same structure as the anatase TiO_2, in agreement with the phase composition determined by PXRD. Inset of Fig. 1b shows the expanded views of E_g Raman band at 147 cm^{-1}. It is found that the E_g band in undoped TiO_2 shifts to the higher wavenumber when S doping, also hinting the incorporation of S into TiO_2 crystal lattice.[11c,12b]

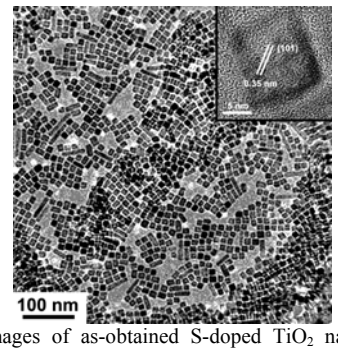

Fig. 2 TEM images of as-obtained S-doped TiO_2 nanocrystals (inset shows the corresponding HRTEM image).

The transmission electron microscope (TEM) measurements shown in Fig. S2† reveal that the TiO_2 nanocrystals obtained from the thermo-decomposition of TiF_4 in OA/OM/ODE solvents without S doping, present irregular morphologies with an average size ranging from 11.8 nm to 25.7 nm, while the S-doped TiO_2 nanocrystals are nearly monodisperse in the size of (14.5±1.2) nm × (15.3±1.1) nm (Fig. 2), indicating S anions can act as a growth controlling agent to produce well-shaped nanocrystals in the current reaction system. However, the sole use of ODE in our synthesis can only yield irregular products (see Fig. S3†). As demonstrated from the energy dispersive X-ray analysis (EDAX) analysis (Fig. S4†), the atomic ratio of Ti:O and is calculated to be 0.49:1 for undoped TiO_2 and 0.53:1 for S-doped TiO_2, respectively, which is in agreement with the stoichiometric ratio of TiO_2. The inset of Fig. 2 is the representative high resolution transmission electron microscopy (HRTEM) image of S-doped TiO_2 nanocrystals that displays evident lattice fringes, indicating the high crystallinity of the as-obtained nanocrystals. The interplanar spacings for the S-doped TiO_2 nanocrystals are calculated to be 0.35 nm, identical to the distances between the (101) crystal planes of anatase TiO_2. It's also worth noting from Fig. 2, the as-obtained S-doped TiO_2 nanocrystals are highly dispersed and exhibit an ordered arrangement, indicative of the retentivity of capping ligands on the surfaces of nanocrystals, as evidenced by Fourier Transform Infrared Spectroscopy (FTIR) measurement results in Fig. S5†.

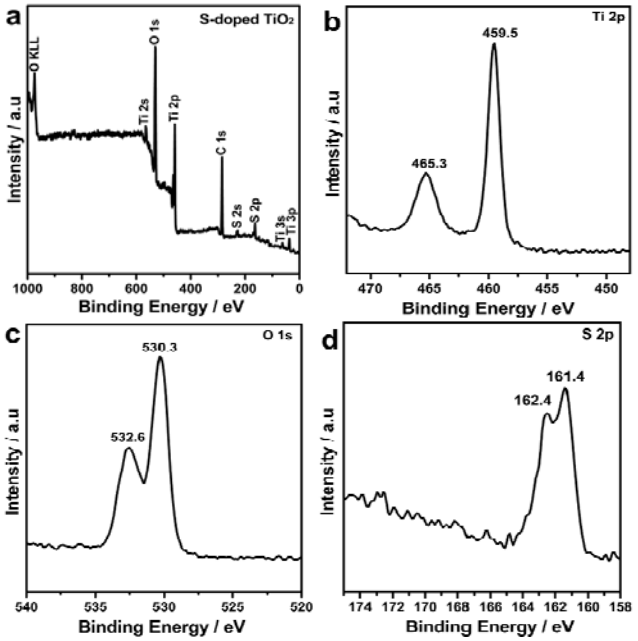

Fig. 3 (a) XPS survey spectra of as-obtained S-doped TiO_2 nanocrystals. (b) Ti 2p, (c) O 1s, and (d) S 2p signals taken from S-doped TiO_2 nanocrystals.

The chemical states of the S-doped TiO_2 nanocrystals have been investigated with X-ray photoelectron spectra (XPS) as shown in Fig. 3. It can be seen from Fig. 3a that the XPS survey spectra shows the S-doped TiO_2 contained predominantly Ti, O, C and S elements. The sharp peaks attributed to the core levels of C 1s reveal the presence of oleic acid and oleylamine ligands on the surfaces of the doped nanocrystals.[19] Panels b-d of Fig. 3 show XPS spectra recorded for the Ti 2p, O 1s, and S 2p regions of the S-doped TiO_2 nanocrystals. As seen from the Fig. 3b, two intense peaks at 465.3 and 459.5 eV ascribed to the core levels of Ti $2p_{1/2}$ and Ti $2p_{3/2}$, respectively, demonstrates that the oxidation states of titanium ions are mainly quadrivalence for the S-doped TiO_2 nanocrystals. The fitting of O 1s region with two peaks shown in Fig. 3c indicates that at least two kinds of oxygen species are existed in the near surface domain of the S-doped TiO_2 nanocrystals. The peak located at about 530.3 eV is due to crystal lattice oxygen of S-doped TiO_2 nanocrystals, while the peak at about 532.6 eV is due to chemisorbed oxygen on the nanocrystal surfaces. Fig. 3d depicts the XPS spectra taken from the S 2p regions for S-doped TiO_2 nanocrystals. Two observable peaks at 162.4 and 161.4 eV attributable to the core levels of S $2p_{1/2}$ and S $2p_{3/2}$, respectively, which are separated by a spin-orbit splitting of 1.0 eV. No evidence of S^{6+} (binding energy at 169.0 eV) is detected, demonstrating the sulfur atoms are all in the state of S^{2-}.[12a,c] It corresponds to the Ti–S bond formed when some of the oxygen atoms in the TiO_2 crystal lattice are replaced by sulfur atoms, as a results of band gap narrowing of TiO_2 calculated by Umebayashi et al.[6c] It is also noted that in our XPS

characterization, we employed the Al-Kα radiation as the X ray light source, the escape depth is around 2 nm (Fig. S6† and S7†). Relative to the sizes of as-synthesized S-doped TiO_2 nanocrystals, the XPS characterization information in our study is also from the total samples.

Fig. S5† exhibits the FTIR spectra of oleic acid, oleylamine, and the prepared S-doped TiO_2 nanocrystals dispersed in toluene/hexane solutions. The strong C–H stretching vibrations at 2920 and 2849 cm^{-1} shows the coexistence of free oleic acid and oleylamine. The observable peak located at 1456 cm^{-1} is ascribed to carboxylate (COO^-) stretch, indicating the COO^- ligands existed on the surface of TiO_2 and S-doped TiO_2 nanocrystals. In addition, the discernible peaks at 1375 cm^{-1} is attributed to the C–N stretch of oleylamine. Based on the FTIR analysis of TiO_2 and S-doped TiO_2 nanocrystals, it is validated that the as-obtained nanocrystals are possibly coated by two kinds of organic molecule, namely oleic acid and oleylamine.[20] Moreover, compared with the pure TiO_2, the new band located at 1045 and 860 cm^{-1} is the characteristic of Ti–S vibration, further indicating the successful doping of S anions into TiO_2 nanocrystals.[11b,13]

Fig. 4a shows the ultraviolet visible (UV-vis) absorption spectrum of as-prepared pure TiO_2 and S-doped TiO_2 nanocrystals dispersed in toluene/hexane solutions. A discernible absorption edge was detected at 385 nm and 415 nm, which is the lowest-energy excitonic absorption peak of TiO_2 and S-doped TiO_2 nanocrystals, respectively. In comparison to the band-gap energy of pure TiO_2, the lowest-energy exciton transition peak of S-doped TiO_2 shows a noticeable red shift, implying that the S dopants are incorporated into the lattice of TiO_2, thus altering its crystal and electronic structures, which enables the S-doped TiO_2 nanocrystals as the effective visible-light photocatalysts.[6c,12b]

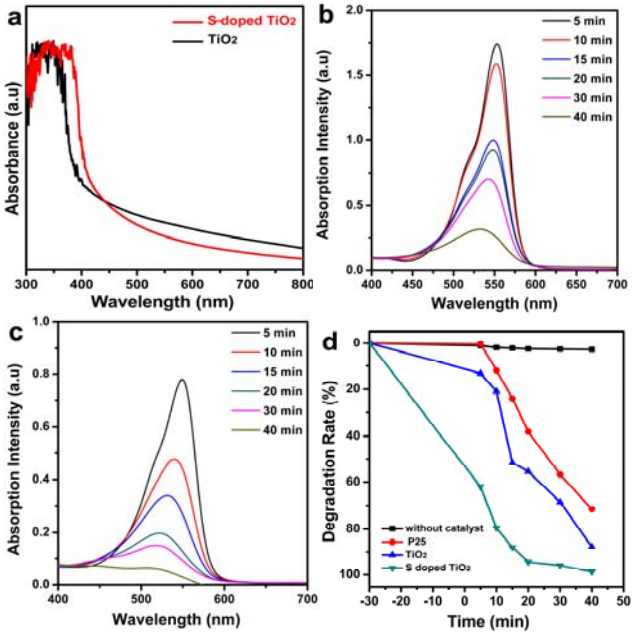

Fig. 4 (a) UV-visible absorbance spectra of pure TiO_2 and S-doped TiO_2 nanocrystals; UV-vis spectra of rhodamine B (RhB) dye vs. photoreaction time in the presence of (b) TiO_2 and (c) S-doped TiO_2 nanocrystals. (d) Photocatalytic degradation of RhB dye over without catalyst, commercial P25, TiO_2 and S-doped TiO_2 nanocatalysts under visible light irradiation (λ = 420–770 nm).

The photocatalytic properties of as-prepared nanocatalysts are studied by photodegradation of rhodamine B (RhB) dye. Fig. 4b and 4c show the change of absorption spectra for the photocatalytic degradation of RhB dye as a function of irradiation time under artificial visible light (λ = 420–770 nm) in the presence of synthesized TiO_2 and S-doped TiO_2 nanocatalysts. The intensity of the absorption band of RhB dye located at λ = 553 nm gradually decrease when prolonging irradiation time, showing that the decoloration of RhB dye can be achieved by TiO_2 and S-doped TiO_2 nanocatalysts under visible-light irradiation. It should be pointed out that the visible-light photocatalytic activity of undoped TiO_2 nanocatalysts may be caused by the concomitant oxygen deficiency.[6f,12b] Compared with the pure TiO_2 shown in Fig. 4b, the RhB dye has almost completely degraded after 40 min under visible light irradiation for S-doped TiO_2 nanocatalysts (Fig. 4c), indicating the S-doped TiO_2 nanocatalysts show the enhanced photocatalytic activity under the same conditions (Fig. S8†).

Fig. 4d shows the photodegradation rate of RhB dye at various time intervals during the visible light irradiation by pure TiO_2 and S-doped TiO_2 nanocatalysts. For comparison, the decomposition over commercial P25 was carried out under the same experimental conditions. As can be seen from the Fig. 4d, S-doped TiO_2 nanocrystals show a superior visible light photodegradation rate of RhB dye to undoped TiO_2 nanocatalysts. Compared with the pure TiO_2 nanocrystals (the degradation rate is 87.5%), the photocatalytic activities and photodegradation rates increase for S-doped TiO_2 nanocrystals with the maximum photocatalytic activity being 99%. In addition, both the as-obtained undoped TiO_2 and S-doped TiO_2 nanocrystals show enhanced degradation rate of RhB dye compared with the commercial P25 (the degradation rate is 70.1%). On the other hand, the adsorption experiments were performed on all catalysts in the absence of light for 30 min. The larger absorption ratio of S-doped TiO_2 nanocrystals may attributed to the higher surface area for them (Fig. 4d).[11a] The photocatalytic stability of the S-doped TiO_2 nanocrystals under visible light irradiation is shown in Fig. S9†. Experimentally, the photocatalysts were used repeatedly six times after separation through filtration, and the activity was evaluated and compared. As can be seen from Fig. S9†, when irradiated by visible light for 15 min, the photocatalytic degradation efficiency of RhB was kept 80% after the sixth time, demonstrating a highly stable photocatalytic performance for as-obtained S-doped TiO_2 nanocatalysts. In addition, we used methylene blue (MB) dye as another model molecule to evaluate the photodegradation performance of as-synthesized S-doped TiO_2 nanocatalysts, as seen from Fig. S10†, the S-doped TiO_2 nanocrystals also show a enhanced visible light photodegradation rate of MB dye to pure P25 and undoped TiO_2 nanocatalysts.

As indicated from the XRD, XPS, FTIR, and UV-vis results, it can be concluded that S was incorporated into the O site of the TiO_2 crystal lattice. In the undoped TiO_2 crystal, the valence band (VB) and conduction band (CB) consist of the Ti 3*d* and O 2*p* orbital. According to the crystal field theory, the Ti 3*d* orbital is split into two parts of the t_{2g} and e_g states in an octahedral field with O_h symmetry, thus the CB is separated into the lower and upper parts. When S doped into TiO_2 crystal, the S 3*p* states are

delocalized, thus playing a significant role in the formation of the VB with the O 2*p* and Ti 3*d* states. As a consequence, the mixing of the S 3*p* states with VB increases the width of the VB, which accounts for the band gap narrowing due to S doping, as illustrated in Fig. S11†.[6c,21]

In summary, in this paper, we have firstly demonstrated a facile synthesis of monodisperse S-doped TiO_2 nanocatalysts in hot boiling organic solvents of oleic/oleylamine/1-octadecene. The as-obtained S-doped TiO_2 nanocatalysts are predominately composed of quadrilateral plate-like shapes, and have an average size in the range of (14.5±1.2) nm × (15.3±1.1) nm. Compared with the as-obtained undoped TiO_2 nanocatalysts, the S-doped TiO_2 nanocatalysts present obvious enhanced visible light activation for the degradation of rhodamine B and methylene blue dyes under the artificial visible light (λ = 420–770 nm) irradiation. We believe that our strategy could be broadly applicable for the facile production of other TiO_2 nanocatalysts doped with nonmetals with great promise for various applications.

Acknowledgements

We gratefully acknowledge the financial aid from the start-up founding from Xi'an Jiaotong University (XJTU), "Nation 1000 Young Talents" program, and the National Nature Science Foundation of China (NSFC, Grant No. 21371140).

Notes and references

[a] *Frontier Institute of Chemistry, Frontier Institute of Science and Technology jointly with College of Science, Xi'an Jiaotong University, 99 Yanxiang Road, Yanta District, Xi'an Shaanxi Province, 710054, China, E-mail: ypdu2013@mail.xjtu.edu.cn; ypdupku@gmail.com; Tel&Fax: 86-29-83395385*

[b] *Key Laboratory of Synthetic and Natural Functional Molecule Chemistry of Ministry of Education, College of Chemistry & Materials Science, Northwest University, Xi'an, Shaanxi, 710069, China.*

[c] *New Energy Research Institute, School of Environment and Energy, South China University of Technology, Guangzhou Higher Education Center, Guangzhou 510006, China.*

† Electronic Supplementary Information (ESI) available: The experimental details, result of FTIR is provided. See DOI: 10.1039/b000000x/

1 A. Fujishima and K. Honda, *Nature*, 1972, **238**, 37.

2 D. F. Ollis and H. Al-Ekabi, Photocatalytic Purification and Treatment of Water and Air, *Elsevier Science*, 1993, 719–725.

3 M. R. Hoffmann, S. T. Martin, W. Choi and D. W. Bahnemann, *Chem. Rev.*, 1995, **95**, 69.

4 M. S. Dresselhaus and I. L. Thomas, *Nature*, 2001, **414**, 332.

5 (a) W. Choi, A. Termin and M. R. Hoffmann, *Angew. Chem., Int. Ed.*, 1994, **33**, 1091; (b) J. A. Wang, R. Limas-Ballesteros, T. Lopez, A. Moreno, R. Gomez, O. Novaro and X. J. Bokhimi, *J. Phys. Chem. B*, 2001, **105**, 9692; (c) I. S. Shah, W. Li, P. C. Huang, O. Jung and C. Ni, *Proc. Natl. Acad. Sci.*, 2002, **99**, 6482; (d) H. Haick and Y. Paz, *J. Phys. Chem. B*, 2003, **107**, 2319; (e) S. Kim, S. J. Hwang and W. J. Choi, *Phys. Chem. B*, 2005, **109**, 24260.

6 (a) R. Asahi, T. Morikawa, T. Ohwaki, K. Aoki and Y. Taga, *Science*, 2001, **293**, 269; (b) S. U. M. Khan, M. Al-Shahry and W. B. Ingler Jr, *Science*, 2002, **297**, 2243; (c) T. Umebayashi, T. Yamaki, H. Itoh and K. Asai, *Appl. Phys. Lett.*, 2002, **81**, 454; (d) S. Sakthivel and H. Kisch, *Angew. Chem. Int. Ed.*, 2003, **42**, 4908; (e) J. C. Yu, W. K. Ho, J. G. Yu, H. Y. Yip, P. K. Wong and J. C. Zhao, *Environ. Sci. Technol.*, 2005, **39**, 1175; (f) W. Ho, J. C. Yu and S. Lee, *Chem. Commun.*, 2006, **10**, 1115; (g) H. Tian, J. F. Ma, K. Li and J. J. Li, *Ceram. Int.*, 2009, **35**, 1289; (h) B. Naik, K. M. Parida and C. S. Gopinath, *J. Phys. Chem. C*, 2010, **114**, 19473.

7 C. Wang, D. W. Bahnemann and J. K. Dohrmann, *Chem. Commun.*, 2000, **16**, 1539.

8 T. Ohno, T. Mitsui and M. Matsumura, *Chem. Lett.*, 2003, **32**, 364.

9 T. Umebayashi, T. Yamaki, S. Tanaka and K. Asai, *Chem. Lett.*, 2003, **32**, 330.

10 L. Gao, S. Zheng and Q. H. Zhang, Nanometer Titania Photocatalytic Materials and Their Applications, *Chemical Industry Press*, 2002, 104.

11 (a) S. X. Liu and X. Y. Chen, *J. Hazardous Mater.*, 2008, **152**, 48; (b) Y. M. Liu, J. Z. Liu, Y. L. Lin, Y. F. Zhang and Y. Wei, *Ceramics Int.*, 2009, **35**, 3061; (c) S. H. Nam, T. K. Kim and J. H. Boo, *Catal. Today*, 2012, **185**, 259.

12 (a) W. Ho, J. C. Yu and S. C. Lee, *J. Solid State Chem.*, 2006, **179**, 1171; (b) G. Liu, C. H. Sun, S. C. Smith, L. Z. Wang, G. Q. Lu and H. M. Cheng, *J. Colloid and Interface. Sci.*, 2010, **349**, 477.

13 G. D. Yang, Z. F. Yan and T. C. Xiao, *Appl. Surface Sci.*, 2012, **258**, 4016.

14 (a) X. W. Wu, D. J. Wu and X. J. Liu, *Appl Phys A*, 2009, **97**, 243; (b) M. V. Dozzi, S. Livraghi, E. Giamellob, E. Selli, *Photochem. Photobiol. Sci.*, 2011, **10**, 343.

15 (a) E. M. Rockafellow, L. K. Stewart and W. S. Jenks, *Appl. Catal. B: Environ.*, 2009, **91**, 554; (b) L. Szatmáry, S. Bakardjieva, J. Šubrt, P. Bezdička, J. Jirkovský, Z. Bastl, V. Brezová and M. Korenko, *Catal. Today*, 2011, **161**, 23.

16 M. Jalalah, M. Faisal, H. Bouzid, A. A. Ismai and S. A. Al-Sayari, *Mater. Res. Bulletin*, 2013, **48**, 3351.

17 H. X. Li, X. Y. Zhang, Y. N. Huo and J. Zhu, *Environ. Sci. Technol.*, 2007, **41**, 4410.

18 (a) T. Ohsaka, F. Izumi and Y. Fujiki, *J. Raman Spectrosc*, 1978, **7**, 321; (b) C. Han, M. Pelaez, V. Likodimos, A. G. Kontos, P. Falaras, K. O'Shea and D. D. Dionysiou, *Appl. Catal. B: Environ.*, 2011, **107**, 77.

19 Y. P. Du, Z. Y. Yin, J. X. Zhu, X. Huang, X. J. Wu, Z. Y. Zeng, Q. Y. Yan and H. Zhang, *Nat. Commun.*, 2012, **3**, 1177.

20 Y. P. Du, Z. Y. Yin, X. H. Rui, Z. Y. Zeng, X. J. Wu, J. Q. Liu, Y. Y. Zhu, J. X. Zhu, X. Huang, Q. Y. Yan and H. Zhang, *Nanoscale*, 2013, **5**, 1456.

21 (a) T. Umebayashi, T. Yamaki, S. Yamamoto, A. Miyashita, S. Tanaka, T. Sumita, and K. Asai, *J. Appl. Phys.*, 2003, **93**, 5156; (b) T. Ohno, M. Akiyoshi, T. Umebayashi, K. Asai, T. Mitsui, M. Matsumura, *Appl. Catal. A-Gen.*, 2004, **265**, 115.